Catalysis Today 155 (2010) 247–254

Contents lists available at ScienceDirect

Catalysis Today

journal homepage: www.elsevier.com/locate/cattod

Morphology induced CO, pyridine and lutidine adsorption sites on TiO_2: Nanoparticles, nanotubes and nanofibers

J.A. Toledo-Antonio *, M.A. Cortés-Jácome, J. Navarrete, C. Angeles-Chavez, E. López-Salinas, A. Rendon-Rivera

Molecular Engineering Division, Instituto Mexicano del Petróleo, Eje Central Lázaro Cárdenas #152, 07730 México, D.F., Mexico

ARTICLE INFO

Article history:
Available online 29 December 2009

Keywords:
Titania anatase
Nanoparticles
Nanotubes
Nanofibers
FTIR of CO adsorption
FTIR of Lutidine adsorption
FTIR of pyridine

ABSTRACT

Anatase with nanotubular (NT) and nanofibrilar (NF) morphology was obtained by annealing treatment at 773 and 873 K of a hydrous titanate with nanotubular morphology synthesized by alkali hydrothermal method. The surface properties were compared with those of a commercial anatase made up of nanoparticles (NPs); materials with similar specific surface area were selected for this end. Low temperature CO adsorption FTIR showed only one adsorption site on the OH groups of nanotubes and nanofibers and almost no Lewis sites were detected suggesting the absence of coordinatively unsaturated Ti^{4+} sites in NT and NF samples. All the OH groups on anatase nanotubes are exposed on the surface, and they are not of Brönsted type. The OH groups in NT and NF adsorb 2.2 times pyridine or lutidine molecules than nanoparticles via H-bonding interaction. These weak interactions are very attractive in the elimination of N-compounds from oil fractions using regenerable adsorbents.

1. Introduction

Semiconductor oxides, such as titanium oxide, have attracted considerable attention because their multiple potential applications in photocatalysis, sensors technology, energy conversion, paints and cosmetics products, corrosion-protective coatings, optical and electronic devises, adsorbents and catalysis [1]. In order to improve photocatalytic and catalytic reactions, a better understanding of the TiO_2 surface properties must be achieved. In fact, among the numerous studies dealing with the surface properties of transition metal oxides by IR spectroscopy, a number of them are devoted to anatase and rutile [2–5].

In general, the surface acidity of titania is of Lewis type, even though some authors have reported the existence of protonic acid sites on anatase [6,7] due to the presence of hydroxyl groups and impurities such as sulfate groups on the surface. Moreover, two kinds of surface hydroxyl groups have been identified on the anatase surface with bands at 3680–3665 and 3740–3710 cm^{-1} [8,9]. Notwithstanding, it has been established that there was no direct relationship between the degree of anatase dehydroxylation and the concentration of the different Lewis acid sites [10]. On the other hand, CO is the most used molecule probe for determination of the strength of protonic acid sites, to characterize both acidic and basic sites of metal oxides. The interaction of CO with surface sites in metal oxides can be classified into three types: (i) with OH groups, (ii) with basic oxygens and (iii) with metal cations [11]. The use of CO molecule as a probe has been exploited for the determination of acid or basic strength of OH groups on metal oxides (12). The OH vibration frequency shift caused by the hydrogen bonding of OH with CO can be related to its Brönsted acidity. Zaki and Knözinger reported that the OH groups were too basic to be perturbed by CO at 78 K [12].

Low temperature CO adsorption allow the detection of a larger number of adsorption sites on anatase surface showing absorption bands at 2175, 2165, 2155 and 2140 cm^{-1}. Accordingly, the bands at 2175 and 2165 cm^{-1} have been attributed to the presence of different kinds of Lewis acid sites related to five-fold coordinated titanium cations situated on different faces (edges, corners, steps) of the anatase crystallites [3,4,6,13], The band at 2155 cm^{-1} characterizes the CO adsorbed on surface hydroxyls groups related to the Brönsted acidity, whereas the band at 2140 cm^{-1} correspond to physically adsorbed CO, thought more recently the later band was associated to the interaction of CO with O^{2-} anions on titania surface [14].

On the other hand, the low specific surface area showed by anatase and rutile polymorphs of titania limit their applications in catalysis. Recently it was demonstrated that anatase or rutile phases of titania can be converted into titanates with nanotubular or nanofibrilar morphology through a relatively simple alkaline hydrothermal method [15,16], yielding hydrous titanate with

* Corresponding author. Tel.: +52 55 91 75 8433.
E-mail address: jtoledo@imp.mx (J.A. Toledo-Antonio).

0920-5861/$ – see front matter © 2009 Elsevier B.V. All rights reserved.
doi:10.1016/j.cattod.2009.11.011

specific surface area as large as 400 m^2/g [17]. However, hydrous titanates are not thermally stable and after annealing at temperatures higher than 673 K, their nanotubular morphology collapse getting back again into nanoparticles of anatase phase [17,18], with the consequent loose of the textural properties. Nevertheless, by an adequate annealing procedure under flowing inert atmosphere, nanotubular hydrous titanate annealed at 673 K is able to maintain the nanotubular structure and the specific surface area as high as 320 m^2/g [19]. At this conditions however, the nanotubular material was composed by a mixture of anatase and titanate phases with tetragonal and orthorhombic structures, respectively. It has been found that nanotubes efficiently disperse transition metal oxides such as WO_3 [20] and V_2O_5 [21] retaining their morphology and textural properties, nevertheless the structure change into anatase after further annealing treatment. Then, an increase in the surface active sites density is expected when used as catalysts in partial oxidation reactions [22]. Additionally, titania nanotubes efficiently disperse metals, such as Pt, Ru, Au and Pd [23–25] showing considerable improvements on their catalytic performance. Considering that titania-supported metals are typical for the observation of the phenomena called "strong metal–support interaction" (SMSI) [26], special attention must be taken on the surface characterization of titania nanotubes.

In this work, surface characterization of the OH groups of strongly anisotropic anatase with nanotubular and nanofibrilar morphology was studied by FTIR of low temperature CO adsorption. Nanotubes and nanofibers of anatase phase were obtained by carefully annealing a hydrous titanate nanotubes at temperatures of 773 and 873 K in dynamic inert atmosphere. CO adsorption sites for anisotropic anatase were compared with those for anatase nanoparticles with nearly the same specific surface area. Additionally, the nature of the OH groups on nanotubes was investigated by FTIR of pyridine and 2,6 dimethylpyridine (lutidine).

2. Experimental

2.1. Preparation of titania materials

Anatase Hombifine N, supplied by Sachtleben Chemie GmbH, was used as a precursor throughout this study. The BET surface area of this sample was 347 m^2/g, and it was 100% anatase, with a crystallite size below ~8.0 nm. Anatase precursor was annealed at 673 and 873 K in order to compare FTIR CO adsorption data. These samples were labeled as NP–*x*, where NP stands for nanoparticles, whereas *x* indicates the annealing temperature.

Nanotubular titania was synthesized by hydrothermally treating the anatase precursor. Forty-five grams of Hombifine N powder were suspended in 3 L of an aqueous 10 M NaOH solution and the resulting suspension was placed in a 4 L autoclave. The hydrothermal reaction was conducted at 373 K, during 18 h under stirring at 200 rpm. Then, the white slurry was filtered and neutralized with a 1 M HCl solution until the pH was lowered to 3.0. The resulting suspension was maintained at this pH overnight under continuous stirring. The material was repeatedly washed with abundant deionized water until it was chlorine-free, i.e. by testing with silver nitrate solution. The material was finally dried overnight at 373 K, yielding a hydrous titania powder with nanotubular morphology. Thereafter, the sample was calcined at 773 and 873 K under dynamic nitrogen flow in a tubular oven for 4 h. Samples were coded as NT-773 and NF-873, where NT means nanotubes and NF nanofibers.

2.2. Characterization

The Raman spectra were recorded using an Yvon Jobin Horiba (T64000) spectrometer, equipped with a confocal microscope (Olympus, BX41) with an Ar ion laser operating at 514.5 nm at a power level of 10 mW. The spectrometer is equipped with a CCD camera detector. Powdered titania nanotubes were placed in a Linkam cell stage directly adapted to the microscope of the instrument, which provides controlled atmosphere and temperature. The glass window of the cell was 1 mm thick.

Textural properties were determined in an ASAP-2000 analyzer from Micromeritics. Specific surface area (SSA) was calculated from Brunauer–Emmet–Teller (BET) equation from N_2 physisorption at 77 K. Pore size distribution was obtained by the Barrett–Joyner–Halenda (BJH) method in the desorption stage. Dried samples were outgassed at 373 K and those calcined at 673 K were outgassed at 623 K.

Transmission electron microscopy was carried out in a JEM-2200FS equipment with accelerating voltage of 200 kV. The microscope is equipped with a Schottky-type field emission gun and an ultra-high resolution (UHR) configuration (Cs = 0.5 mm; Cc 1.1 mm; point-to-point resolution, 0.19 nm) and in-column energy filter omega-type. The samples were ground, suspended in isopropanol at room temperature, and dispersed with ultrasonic stirring; then, an aliquot of the solution was dropped on a 3 mm diameter lacey carbon copper grid.

Transmission infrared (IR) spectra were recorded using a Nicolet Fourier Transform infrared (FTIR), Protégé-460 spectrophotometer at a spectral resolution of 2 cm^{-1} accumulating 128 scans, in a self-supported disk. The IR cell was connected to a vacuum/sorption system capable of temperature control with a residual pressure below 0.133 Pa. The cell allowed recording the IR spectra at 100 K. The self-supported 0.01–0.02 g disk, made of compressed sample at 490 MPa, was thermally treated *in situ* in the IR cell, under vacuum at 673 K, before exposing it to CO, pyridine or 2,6 dimethylpyridine (lutidine). For CO adsorption, a large amount of CO (~2.6 kPa) was admitted on the samples cooled at 100 K. Then, the excess of CO was evacuated, by decreasing the pressure to 0.133 Pa. Pyridine or lutidine adsorption was done at 298 K. A relatively large excess of pyridine or lutidine (~50 μL) was admitted on the samples, and thereafter, the excess of pyridine or lutidine was evacuated at 323 K, and the reported FTIR spectra were recorded at these conditions. All FTIR spectra were normalized to the sample weight.

3. Results and discussion

3.1. Structure

Anatase nanoparticles (NPs samples) annealed at 673 and 873 K, showed Raman spectra with very intense vibrating bands at 144, 200, 396, 505, 640 cm^{-1}, characteristic of the anatase phase [27], as shown in Fig. 1. The nanostructured samples, i.e. nanotubes and nanofibers (NT-773 and NF-873) obtained from nanotubular titanates annealed at 773 and 873 K, showed exactly the same bands with lower intensity than that of NP samples. Besides anatase, no evidence of another structure, e.g. titanates or rutile, was observed, suggesting that all the initial titanates were transformed into anatase phase, in agreement with the literature [18,24]. Accordingly, at temperatures above 673 K, titanate nanotubes transform into anatase nanofibers. Nevertheless, in our recent study [19] titanate nanotubes annealed at 673 K did not completely transform into anatase, so we selected 773 and 873 K temperatures in order to have a titania with nanotubular and nanofibrilar morphology, respectively, completely transformed into anatase, as can be noted in Fig. 1.

3.2. Morphology

The morphology of the samples was examined by TEM, where the anatase precursor (NP sample) annealed at 673 K showed well

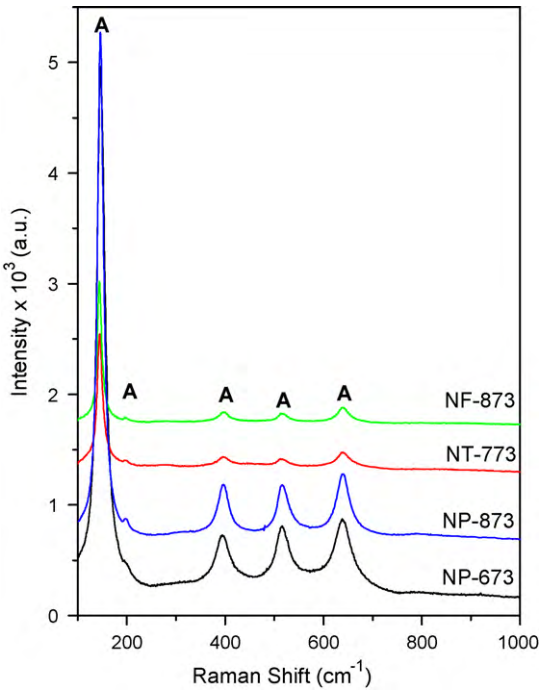

Fig. 1. Raman spectra of anatase nanoparticles, nanotubes and nanofibers annealed at indicated temperature.

defined 5–10 nm nanoparticles as shown in Fig. 2a, with anatase phase confirmed by the electron diffraction pattern (EDP) analysis, Fig. 2b. After converting anatase nanoparticles into titanate nanotubes and then annealing at 773 K, the walls of the nanotubes are made up of anatase phase (see Fig. 3a), where well aligned bundles of nanotubes appeared. An isolated nanotube can be observed in the inset in Fig. 3b, with inner diameter ~8.0 nm and wall thickness ~4.0 nm. These results are in agreement with our Raman results; the walls consist of anatase phase. This information was corroborated by the reflection analysis of the EDP obtained from nanotubes see Fig. 3c. The EDP corresponds to anatase phase.

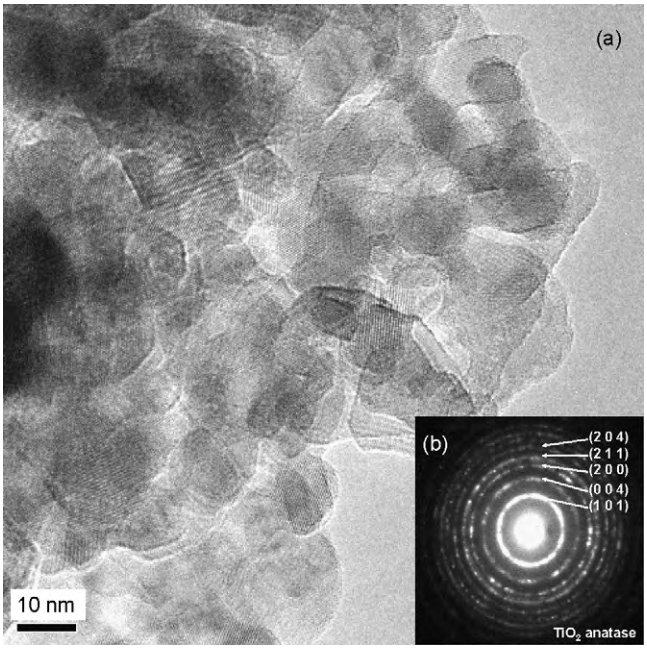

Fig. 2. (a) Transmission electron microscopy of anatase nanoparticles annealed at 673 K and (b) inset electron diffraction pattern.

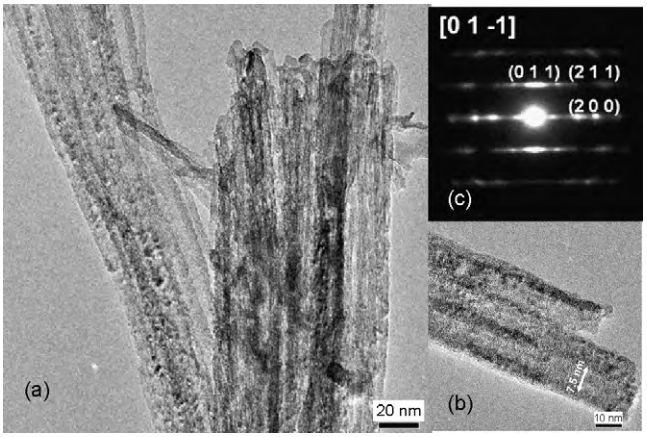

Fig. 3. (a) Transmission electron microscopy of anatase nanotubes annealed at 773 K, (b) detail of an isolated nanotube and (c) electron diffraction pattern.

Structural analysis indicates that the anatase nanotube seem to be aligned along the [0 1 0] direction such as the nanotube precursor. It is important to mention that the nanotubular anatase was the main morphology observed with purity higher than 95% of the explored area.

After annealing at 873 K, anatase nanotubes collapsed and transformed into nanofibers as shown in Fig. 4a. In fact in some regions the nanofibers transformed into nanoparticles of anatase (see inset c and d in Fig. 4). The abundance of the anatase nanofibers in this sample was roughly higher than 80%.

Strongly anisotropic anatase phase with nanofibrilar morphology, that is, perpendicular to the (2 0 0) plane, as shown in Fig. 4b, was produced after annealing at 873 K. In contrast, in the region where the nanotubular structure collapsed into nanoparticles (see Fig. 4c) a typical o-ring EDP corresponding to small nanoparticles was obtained. The diffraction o-rings correspond strongly to anatase phase, as can be seen in Fig. 4d.

3.3. Textural properties

N_2 physisorption isotherms for NP, NT and NF anatase with different morphologies, are shown in Fig. 5. In all materials, type IV isotherms from BDDT classification were observed, characteristic of porous solids [28]. NT and NF anatase showed higher N_2

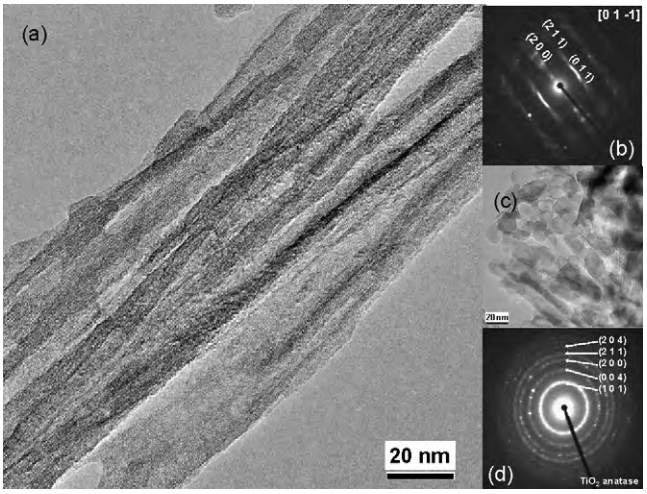

Fig. 4. (a) Transmission electron microscopy of anatase nanofibers annealed at 873 K, (b) electron diffraction pattern of anisotropic anatase, (c) transmission electron microscopy of a collapsed region and (d) electron diffraction pattern of nanoparticles of (c) image.

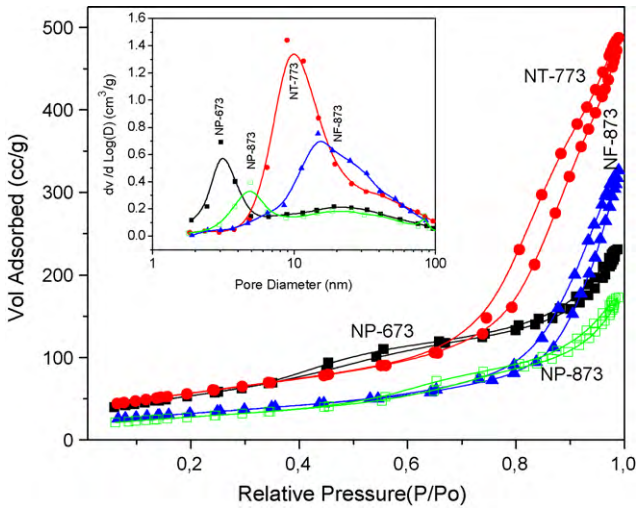

Fig. 5. Adsorption–desorption isotherms and (inset) pore size distribution of indicated anatase materials.

adsorbed volume than nanoparticles. Also the hysteresis loop shifted towards higher relative pressure for NT and NF than that for NP anatase, suggesting an increase in pore diameter, as shown in inset of Fig. 5, where the pore size distribution show that NP anatase has a bimodal porosity of ~3 nm and another less populated one of ~20 nm. NT anatase showed the highest porosity with a pore size centered at 10 nm, which nearly correspond to the inner diameter, measured from the isolated nanotube presented in Fig. 3b. Additionally, a shoulder can be appreciated at 30–40 nm, associated to the pores between the nanotubes originated from the agglomeration or intercrossing of them. In NF anatase, the porosity shifted toward a high pore diameter centered at 20 nm and tailing toward higher diameter as consequence of the nanotubular collapsing, then, this porosity likely arise from the external pores generated by the disordered intercrossing of the nanofibers or bundles of them.

The textural parameters for different TiO_2 morphologies are listed in Table 1. Nanotubular anatase showed the largest SSA (203 m^2/g), quite similar to that of NP anatase annealed at 673 K (196 m^2/g). However, NT and NF showed both a higher pore volume and average pore diameter than NP anatase, which are important parameters to take into account when used as a catalyst support to disperse high loads of non-porous active phases such as metals or transition metal oxides. As reported previously, NT sample annealed at 673 K showed an SSA as high as 321 m^2/g, when it is not completely transformed into anatase [19], then, in this work, in order to compare the influence of the morphology of anatase on the adsorptive properties, different temperatures were selected to have nearly similar SSA in NP and NT or NF samples, that is, 673 and 873 for NP samples and 773 and 873 for NT and NF samples, respectively.

From the above results it is clear that after annealing both titania nanotubes and titania nanoparticles (e.g. the precursor) at 773 and 673 K, mainly anatase phase with different morphological features are obtained: nanotubes and nanoparticles, respectively. Obviously, anatase nanoparticles in the precursor must expose a larger amount of edges, corners and steps sites than those presented in anatase embedded into the walls of a nanotubular morphology. Hence, in the following section, CO adsorption will be used in order to characterize the influence of morphology of anatase nanoparticles, embedded in nanotubes and completely transformed into nanofibers, by annealing nanotubes at temperatures up to 773 K.

Table 1
Textural properties of titania anatase with different morphology.

Sample	Specific area (m^2/g)	Pore volume (cm^3/g)	Avg. pore diameter (nm)
NP-673	196	0.33	5.6
NP-873	102	0.24	9.6
NT-773	203	0.71	11.5
NF-873	116	0.47	14.3

3.4. FTIR spectra comparison

FTIR studies of low temperature CO adsorption on anatase and rutile titania have been investigated previously [4,5], and more recently on nanotubular titania [19]. In our work, the influence of the morphology of anatase phase on the CO adsorption is compared. First, let us discuss the FTIR spectra (see Fig. 6) of anatase nanoparticles annealed at 673 K, which show in the ν(OH) region two main bands at 3702 and 3662 cm^{-1}, characteristic of OH stretching modes of two different types of hydroxyls groups on the anatase surface [4,6,8,9,13]. Additionally at 873 K, two well defined ν(OH) bands shifted to a higher position, that is, 3749 and 3676 cm^{-1}, in comparison with those of NP sample annealed at 673 K. Accordingly, two kinds of hydroxyl groups exist on anatase surface as reported by several authors [2,6,29]. On titania nanotubes and nanofibers surface (NT and NF samples) also the two hydroxyl groups were observed shifted to higher wavenumbers, that is, 3710 and 3668 and 3720 and 3670 cm^{-1} for NT and NF, respectively, suggesting more basic OH groups, than those in NP-673 sample (see Fig. 6). As the spectra were normalized to equal sample's weight, the lower intensity of ν(OH) bands as compared with those of anatase nanoparticles, indicate a lower population of OH groups on NT and NF surface. Other common bands in both samples occurred at 1260 cm^{-1}, which are associated to Ti–O vibrating bands. In anatase NP surface, two bands at 1520 and 1428 were more prominent than on those on nanotubes, which might be attributed to sulfate impurities [30] on the Hombifine N precursor obtained from the

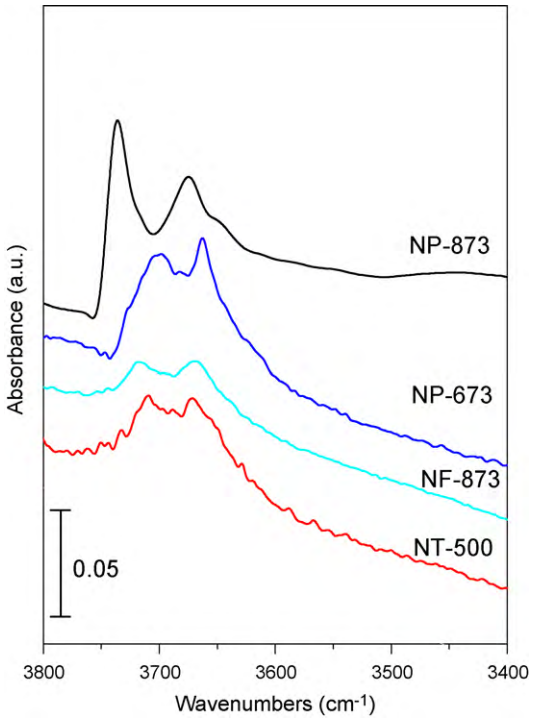

Fig. 6. FTIR of OH region of anatase materials.

sulfate process. The amount of the impurities decreased in the process of the nanotubes transformation.

3.5. Low temperature CO adsorption

Differential FTIR of CO adsorbed at 100 K on NP, NT and NF anatase samples are shown in Fig. 7. In NP-673 sample, after CO exposure at 100 K, a negative band was observed in the ν(OH) region at 3705 cm^{-1}, whereas two more intense peaks occurred at a lower position, e.g. 3554 and a broad band between 3100 and 3050 cm^{-1}. The first one, as consequence of H-bonded CO to surface OH groups, e.g. –O–H ↔ CO interaction, giving rise to an increased in both characteristics intensity and full width at half maximum, as indicated elsewhere [31]. The ν(OH) frequency shift was estimated to *ca.* −149 cm^{-1} and evacuation of CO at higher temperature brings about the disappearance of the 2154 cm^{-1} band, with the consequent restoration of the original hydroxyl groups. The second broad band between 3100 and 3050 cm^{-1} can be attributed to the stretching mode of hydroxyl groups in water molecules with its corresponding bending mode at 1630 cm^{-1}. The bands at 1558 and 1370 cm^{-1} correspond to symmetric and antisymmetric stretching modes of adsorbed formate (HCOO) species [32]. However, a shoulder at 1330 cm^{-1} suggests the presence of bidentate CO_3 adsorbed species which cannot be disregarded [33].

FTIR bands around 1630, 1450–12, 1344–10 cm^{-1} also characterize the ν_{as} (CO), ν_s (CO) and δ(O–H...O) modes of bicarbonate species, respectively [34]. On the basis of these results, it can be concluded that at least one CO portion are oxidized by reacting with OH groups yielding formate, bicarbonate and carbonate species on the anatase surface with the consequent water formation, even at low temperature CO adsorption. It is worth noting that after CO adsorption and evacuation at room temperature, the NP-673 sample turns blue, suggesting the formation of Ti^{3+}. Oxidation of CO has been observed on TiO_2 rutile surface [5] and the appearance of these formate or carbonate species contribute to block the CO adsorption sites.

In CO adsorption on NP-873 (see Fig. 7), no formation of water or any formate or carbonate adsorbed species were observed, indicating a low reactivity of the hydroxyl groups compared with the other samples; the vibrating bands of hydroxyl groups shifted towards higher frequencies compared with those of the corresponding NP-673 sample (see Fig. 6), suggesting a higher basicity of NP-873 sample. However, the ν(OH) red-shift was estimated to be −196 cm^{-1} taking into account the unperturbed ν(OH) at 3740 cm^{-1}, which means a higher acid strength. These results indicates that stronger acid sites are formed upon dehydroxylation of anatase at 873 K than those formed by dehydroxylation at 673 K in agreement with Primet et al. results [35]. Nevertheless, the higher the reactivity of OH groups, the lower the dehydroxylation temperature.

It has been assumed that CO adsorption or acid site density strongly depend on the anatase morphology, although to our knowledge this is the first time that CO is adsorbed on strongly anisotropic anatase in nanotubular and nanofibers morphologies. Then, let us first refer to the hydroxyls and carbonate species. As can be observed in Fig. 7, a portion of CO introduced at very low temperature (100 K) evolve into carbonates (CO_3) or formates (HCOO), characterized by small bands at 1330, 1566 and 1608 cm^{-1}, by reacting with a portion of the hydroxyl groups on the surface of the nanotubular and nanofibers anatase, with the

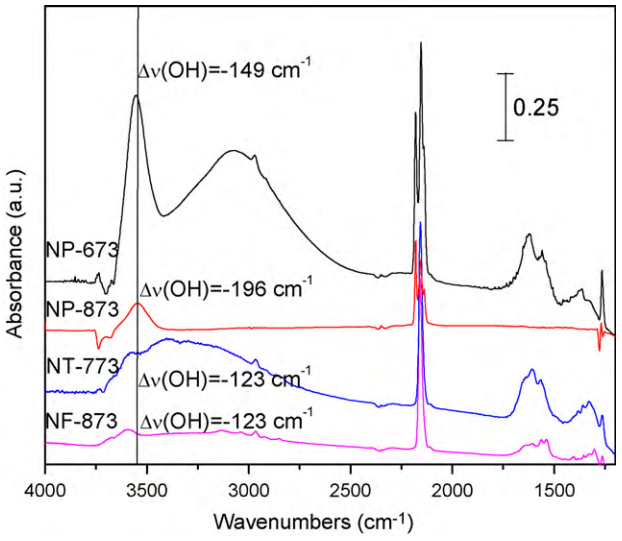

Fig. 7. CO adsorption differential FTIR spectra of anatase materials.

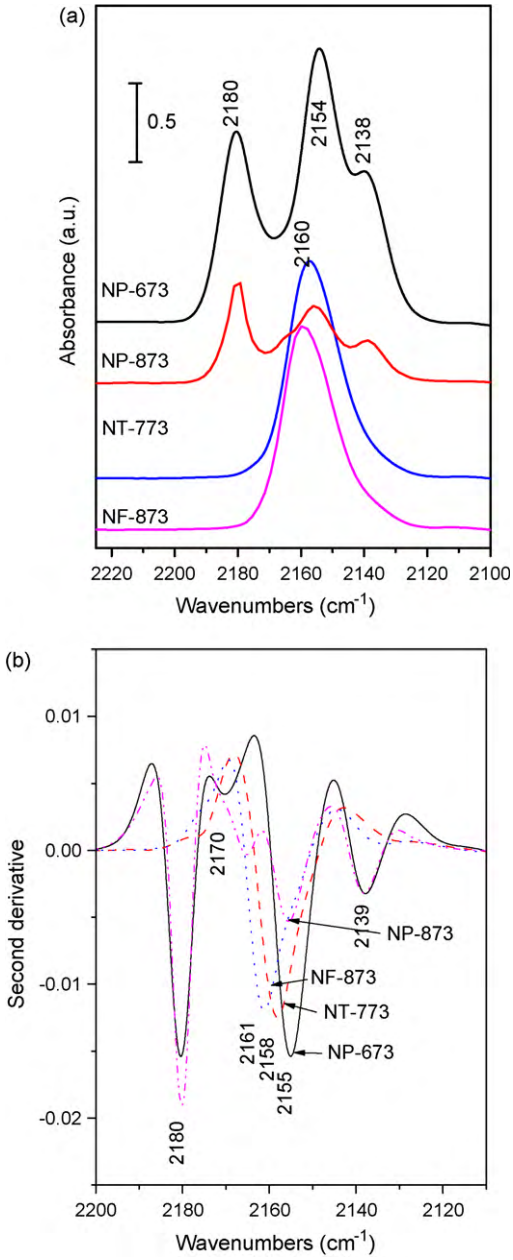

Fig. 8. (a) CO adsorption FTIR spectra of anatase materials. (b) 2nd derivative CO adsorption FTIR spectra of anatase materials.

consequent formation of adsorbed water molecules evidenced by a broad signal at 3500–3000 cm^{-1} and its corresponding bending band at 1637 cm^{-1}. The intensity of the bands associated to carbonates and water strongly depend on the annealing temperature, i.e. the higher the temperature, the lower the OH reactivity. In contrast to the four CO absorption peaks commonly reported and observed for anatase or rutile [4,5,12], only one CO peak around 2158 cm^{-1} occurred, accompanied with the appearance of a broad band from perturbed ν(OH) at 3585 cm^{-1} indicating that this unique CO adsorption sites are hydroxyl groups.

The formation of different CO adsorption sites, depending on the anatase morphology, can be evidenced in Fig. 8. On NT and NF samples, only one kind of CO absorption band was observed, corresponding to the CO adsorption on Ti–OH sites. No CO on coordinatively unsaturated Ti^{4+} sites neither physically adsorbed CO nor the interaction of CO with O^{2-} ions were observed [14]. These results suggest that anatase nanotubes and nanofibers do not expose coordinative unsaturated Ti^{4+} sites and basic O^{2-} anions on its surface, contrary to what is observed on anatase NP samples, where four absorption bands can be noted from the second derivative CO adsorption spectra (see Fig. 8b). Here, the bands at 2180 and 2170 cm^{-1} correspond to CO adsorption on different kinds of Lewis acid sites, indicating the presence of four-fold or five-fold coordinated Ti^{4+} cations situated on the edges, corners or steps of the anatase crystallites [3,4,6,36]. The CO absorption band at 2155 cm^{-1} correspond to CO adsorption on hydroxyls groups as discussed above, and the band at 2139 cm^{-1}, is generally attributed to physically adsorbed CO [4,5,37–39]. The fact that physically adsorbed CO did not occur on NT and NF samples prove the hypothesis that this band correspond to the CO interaction with surface O^{2-} anions, as recently formulated by Hadjjivanov et al. [14], which are exposed only at the surface of anatase nanoparticles.

3.6. Pyridine adsorption

Water is a basic molecule stronger than CO. Hence, the presence of water might perturb the measurement of acidity by CO, since Lewis sites interact with water molecules transforming into Brönsted sites. Therefore, in order to better probe the presence or absence of Lewis sites in Nanotubes, FTIR of pyridine adsorption was carried out on NT-773 and NP-673 samples. FTIR of pyridine adsorption on NT-773 and NP-673 samples is shown in Fig. 9. At room temperature, a larger amount of pyridine molecules are retained on anatase nanoparticles, NP-673 sample, than on nanotubular NT-773 sample, and after pyridine evacuation at 473 K, when practically all weakly bonded or physisorbed pyridine is eliminated, pyridine remain coordinated on the Lewis acid sites of anatase nanoparticles whereas practically no pyridine remain adsorbed on the surface of nanotubes. This result, strongly point out the absence of Lewis acid sites on nanotubes, as previously observed on our CO adsorption experiments.

By analyzing the 8a ring vibrating mode region of pyridine adsorbed at room temperature in Fig. 10, it can be appreciated that pyridine molecules are coordinated in different kind of sites, clearly distinguishable among them, depending on the nature and morphology of the anatase samples, i.e. on NT-773 samples, the main absorption peak appeared at 1591 cm^{-1}, corresponding to 8a ring vibration mode of a H-bonded pyridine [40–42] whereas in NP-673 samples, the main peak occurred at 1603 cm^{-1}, suggesting that pyridine molecules are mainly coordinated to Lewis acid sites [42,43]. Other less intense band occurred at 1575 cm^{-1} on both samples corresponding to physisorbed pyridine and one additional band at 1615 cm^{-1} from protonated pyridinium ion on acidic OH Brönsted sites on NT-773 sample. As FTIR spectra in Fig. 10, were weight normalized and since both NP-673 and NT-773 samples have quite similar SSA, the total amount of H-bonded pyridine can be estimated by deconvolution and area integration of the peaks at 1591 cm^{-1}, in both samples. The H-bonded pyridine adsorbed on titania nanotubes is approximately 2.2 times that on titania nanoparticles, indicating that pyridine interact mainly via OH groups on the surface of nanotubes, whereas in nanoparticles pyridine molecules coordinate mainly via acid–base interaction with the Lewis acid sites. For adsorption application purposes, strong interactions between organic bases and a given adsorbent (i.e. through Lewis sites) are not desirable since regeneration (e.g. easy removal of the adsorbed organic bases) of the adsorbent is a valuable characteristic for economic and environmental reasons.

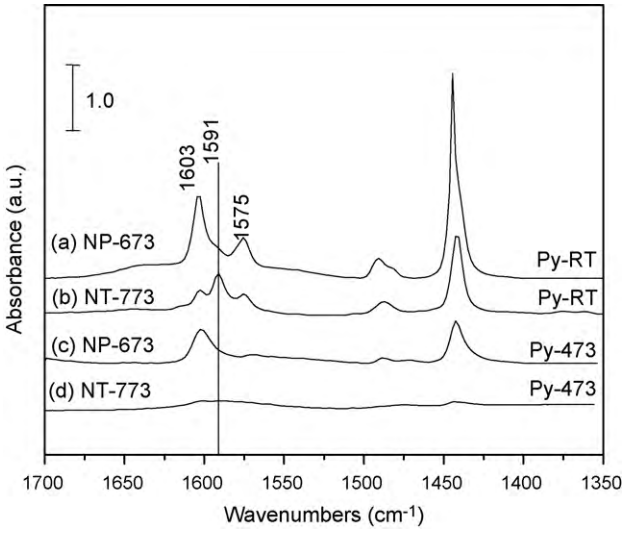

Fig. 9. Pyridine adsorption FTIR spectra of anatase materials. (a) pyridine evacuated at room temperature on NP-673 sample, (b) pyridine evacuated at room temperature on NT-773 sample, (c) pyridine evacuated at 473 K on NP-673 sample and (d) Pyridine evacuated at 473 K on NT-773 sample.

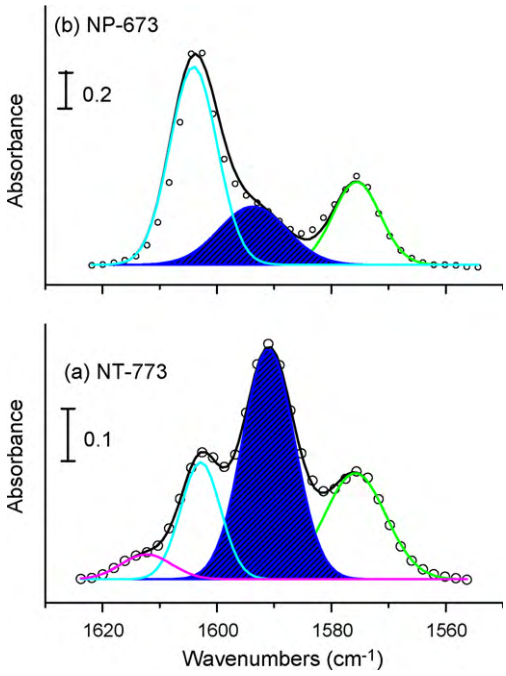

Fig. 10. Pyridine adsorption (8a ring vibrating mode region) FTIR of anatase materials: (a) NT-773 and (b) NP-673 samples (evacuated at room temperature). Shaded peaks correspond to H-bonded weakly interacting pyridine.

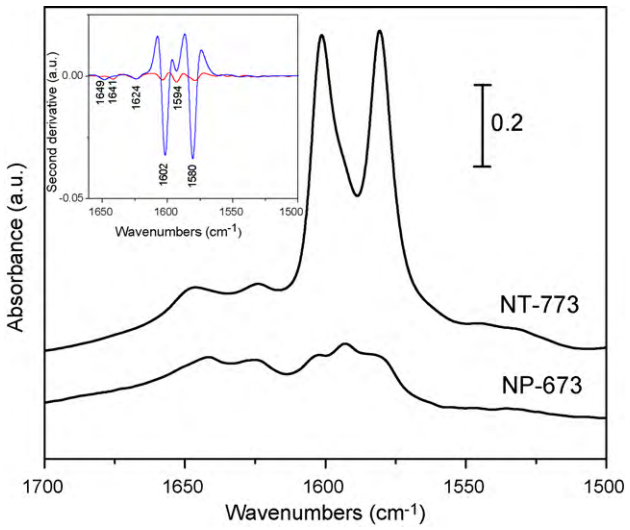

Fig. 11. Lutidine adsorption FTIR spectra of anatase materials. Inset: 2nd derivative curves of lutidine adsorption FTIR spectra.

3.7. Lutidine adsorption

In order to determine the accessibility and nature of the OH groups on the nanotubes surface, FTIR adsorption of 2,6 dimethylpyridine (lutidine) was carried out at 313 K. This molecule contains two methyl groups in the 2- and 6-position, and then the formation of coordinative chemisorption bonds is sterically hindered, playing an important role as a proton probe nature of OH groups on metal oxide systems [44]. In fact, lutidine is considered a more sensitive molecule to characterize Brönsted acidity than pyridine. Therefore, lutidine was used to examine the exact nature of OH groups on the surface of titania nanotubes, since Lewis acidity was not detected by low temperature CO adsorption in this study. FTIR spectra of lutidine adsorbed on titania nanotubes and nanoparticles in the wavelengths range 1500–1700 cm^{-1}, where the 8a and 8b ring stretching modes occur with higher spectral change upon adsorption, is presented in Fig. 11 [45]. Since all FTIR spectra presented in Fig. 11 are normalized to sample weight, it is clear that nanotubes (NT-773) adsorb a higher amount of lutidine than nanoparticles (NP-673). The second derivative plot of adsorbed lutidine spectra is presented in order to distinguish the exact position of the vibrating bands (see inset in Fig. 11). In NT-773 sample, a strong band at 1580 cm^{-1} occur due to the 8b mode of a H-bonding interacting lutidine molecules with its corresponding 8a vibrating mode of the peak at 1602 cm^{-1} of a stronger form of adsorbed lutidine [45], that is, lutidine interacting by H-bonding with the OH groups of the surface of nanotubes, as no Lewis acid sites were detected by CO adsorption. Another less intense band at 1594 cm^{-1} in the second derivative plot is attributed to the 8a mode of physisorbed lutidine molecules, its corresponding 8b mode overlap with the 8b mode of H-bonding lutidine (i.e. ~1580 cm^{-1}). Same interacting lutidine bands were observed on anatase nanoparticles (NP-673 sample) nearly at the same positions as those of NT-773 sample, but less intense, corresponding to the H-bonding and physisorbed lutidine.

In the case of anatase nanoparticles a considerable amount of Lewis sites was detected by low temperature CO adsorption, the 8a vibrating mode slightly shifted at 1604 cm^{-1} could be also attributed to Lewis sites that occur from 1604 to 1615 cm^{-1} depending on the acid strength. However, lutidine molecule has weak interaction with Lewis sites due to the steric hindrance of the methyl groups [44,46], then, we can assume that lutidine vibrating band at 1604 cm^{-1} in NP-673 sample is mainly attributed to H-bonded lutidine on OH groups of anatase nanoparticles surface.

Other two less intense bands at 1649 and 1624 cm^{-1} on titania nanotubes (NT-773) arise from the 8a and 8b modes, respectively of lutidinium ions, characteristic of Brönsted acidity [46]. Same lutidinium ions bands were observed on titania nanoparticles (NP-673) with practically the same intensity (see Fig. 11). The 9b vibrating mode of lutidinium ions remains at the same position in both nanoparticles and nanotubes, whereas the 8a mode shifted from 1641 to 1649 cm^{-1} for nanoparticles and nanotubes samples, respectively; the 8a vibrating mode is sensitive to the acid strength, indicating a higher Brönsted acid strength in nanotubes than in nanoparticles [44–46]. As both samples, NP-673 and NT-773 are made up by anatase phase (see Raman results in Fig. 1), with nearly the same SSA (see Table 1), the difference in Brönsted acidic strength can be correlated to the difference in morphology. A stronger interaction is expected between lutidine and protons exposed on the curved nanotubular surface than that in a flat one, i.e. the steric hindrance conferred by the two methyl groups are reduced by interaction with a protruding proton on a curved nanotubular structure.

As the FTIR spectra in Fig. 11 are normalized to sample weight and both NP-673 and NT-773 samples have quite similar SSA, the total amount of lutidine (H-bonding, physisorbed and Brönsted-bound) adsorbed on the surface of titania nanotubes is approximately 2.25 times that on titania nanoparticles, indicating that nanotubes possesses more accessible OH groups adsorption sites than nanoparticles. Lutidine interaction was given mainly via H-bonding with the OH groups exposed on the surface of titania nanotubes, suggesting that a slightly stronger adsorbate/adsorbent interaction occurs on titania nanotubes. These results are in agreement with the above pyridine discussion.

4. Conclusions

Morphological (nanotubes, nanofibers and nanoparticles) changes in anatase TiO_2 in the nanoparticle range bring about significant variations in the surface physicochemical properties. Two adsorption probes, CO and lutidine indicate that O^{2-} anions and coordinatively unsaturated Ti^{4+} sites behave differently depending on the morphology of anatase. For instance, nanotubes and nanofibers do not expose coordinatively unsaturated Ti^{4+} or basic O^{2-} sites, which occur on nanoparticles. On the other hand, lutidine and pyridine adsorption indicate that Ti–OH groups in nanotubes are 2.25 times more populated in nanotubes than in nanoparticles. The greater accessibility to this OH groups is likely derived from the particular topography of the nanotubes, e.g. a greater number of curved surfaces.

The removal of nitrogen-containing compounds in oil fractions is of up most importance since these bases hamper the activity in various catalytic processes. With a view to develop a commercial regenerable adsorbent, it is necessary that the interaction between the organic base and the adsorbent be a weak one. In this sense, the weak interaction of organic bases such as pyridine and lutidine on anatase, nanotubes and/or nanofibers are a very attractive feature for such applications.

References

[1] U. Diebold, Surf. Sci. Rep. 48 (2003) 53.
[2] L. Yi, G. Ramis, G. Busca, V. Lorenzelli, J. Mater. Chem. 4 (1994) 175.
[3] K. Tanaka, J.M. White, J. Phys. Chem. 88 (1984) 4708.
[4] K. Hadjiivanov, J. Lamotte, J.C. Lavalley, Langmuir 13 (1997) 3374.
[5] K. Hadjiivanov, Appl. Surf. Sci. 135 (1998) 331.
[6] G. Busca, H. Saussey, O. Saur, J.C. Lavalley, V. Lorenzelli, Appl. Catal. 14 (1985) 245.
[7] K. Morishige, F. Kanno, S. Ogawara, S. Sasaki, J. Phys. Chem. 89 (1985) 4404.
[8] G. Spoto, C. Morterra, L. Marchese, L. Orio, A. Zecchina, Vacuum 41 (1990) 37.
[9] V. Bolis, B. Fubini, E. Garrone, C. Morterra, P. Ugliengo, J. Chem. Soc., Faraday Trans. 88 (1992) 391.
[10] C. Morterra, J. Chem. Soc., Faraday Trans. 1 (84) (1988) 1617.
[11] J.C. Lavalley, Catal. Today 27 (1996) 377.

[12] M.I. Zaki, H. Knözinger, Mater. Chem. Phys. 17 (1987) 201.
[13] K. Hadjiivanov, O. Saur, J. Lamotte, J.C. Lavalley, Z. Phys. Chem. 187 (1994) 281.
[14] K. Hadjiivanov, A. Penkova, M.A. Centeno, Catal. Commun. 8 (2007) 1725.
[15] T. Kasuga, M. Hiramatsu, A. Hoson, T. Sekino, K. Niihara, Langmuir 14 (16) (1998) 3160.
[16] G.H. Du, Q. Chen, R.C. Che, Z.Y. Yuan, L.M. Peng, Appl. Phys. Lett. 79 (2001) 3702.
[17] J. Escobar, J.A. Toledo, M.A. Cortés, M.L. Mosqueira, V. Perez, G. Ferrat, E. López-Salinas, E. Torres, Catal. Today 106 (2005) 222.
[18] D.V. Bavykin, J.M. Friedrich, A.A. Lapkin, F.C. Walsh, Chem. Mater. 18 (2006) 1124.
[19] J. Toledo Antonio, S. Capula, M.A. Cortés-Jácome, C. Angeles-Chávez, E. López-Salinas, G. Ferrat, J. Navarrete, J. Escobar, J. Phys. Chem. C 111 (2007) 10799.
[20] M.A. Cortes-Jacome, M. Morales, C. Angeles Chavez, L.F. Ramirez Verduzco, E. López-Salinas, J.A. Toledo Antonio, Chem. Mater. 19 (2007) 6605.
[21] J. Liu, Y. Fu, Q. Sun, J. Shen, Microporous Mesoporous Mater. 116 (2008) 614.
[22] G.C. Bond, J. Sarkany, G.D. Parfitt, J. Catal. 57 (1979) 476.
[23] D.V. Bavykin, A.A. Lapkin, P.K. Plucinski, J.M. Friedrich, F.C. Walsh, J. Catal. 235 (2005) 10.
[24] D.V. Bavykin, A.A. Lapkin, P.K. Plucinski, L. Torrente-Murciano, J.M. Friedrich, F.C. Walsh, Top. Catal. 39 (2006) 151.
[25] L. Torrente-Murciano, A.A. Lapkin, D.V. Bavykin, F.C. Walsh, K. Wilson, J. Catal. 245 (2007) 272.
[26] G.L. Haller, D.F. Resasco, Adv. Catal. 36 (1989) 173.
[27] S. Kelly, F.H. Pollak, M. Tomkiewicz, J. Phys. Chem. B 101 (1997) 2730.
[28] S. Brunauer, L.S. Deming, W.E. Deming, E. Teller, J. Am. Chem. Soc. 38 (1940) 1723.
[29] G. Ramis, G. Busca, V. Lorenzelli, J. Chem. Soc., Faraday Trans. 1 (83) (1987) 1591.
[30] T. Jiang, Q. Zhao, M. Li, H. Yin, J. Hazard. Mater. 159 (2008) 204.
[31] C. Pazé, S. Bordiga, C. Lamberti, M. Salvalaggio, A. Zecchina, J. Phys. Chem. 101 (1997) 4740.
[32] L.F. Liao, W.C. Wu, C.Y. Chen, J.L. Lin, J. Phys. Chem. B 105 (2001) 7678.
[33] L.F. Liao, C.F. Lien, D.L. Shieh, M.T. Chen, J.L. Lin, J. Phys. Chem. B 106 (2002) 11240.
[34] G. Busca, V. Lorenzelli, Mater. Chem. 7 (1982) 89.
[35] M. Primet, P. Pichat, M.V. Mathieu, J. Phys. Chem. 75 (1971) 1216.
[36] K. Hadjiivanov, D. Klissurski, Chem. Soc. Rev. 25 (1996) 61.
[37] T. Tabakova, F. Boccuzzi, M. Manzoli, J.W. Sobczak, V. Idakiev, A. Andreeva, Appl. Catal. A: Gen. 298 (2006) 217.
[38] I. Salla, T. Montanari, P. Salangre, Y. Cesteros, G. Busca, Phys. Chem. Chem. Phys. 7 (2005) 2526.
[39] K. Hadjiivanov, G. Vayssilov, Adv. Catal. 47 (2002) 347.
[40] D. Cook, Canad. J. Chem. 39 (1961) 2009.
[41] E.P. Parry, J. Catal. 2 (1963) 371.
[42] G. Ertl, H. Knözinger, J. Weitkamp, Handbook of Heterogenous Catalysis, VCH Verlagsgesellschaf mbH, Germany, 1997.
[43] K. Nakamoto, Infrared Spectra of Inorganic and Coordination Compounds, Wiley Interscience, New York, 1986.
[44] A. Corma, C. Rodellas, V. Fornes, J. Catal. 88 (1984) 3.
[45] C. Morterra, G. Cerrato, G. Meligrana, Langmuir 17 (2001) 7053.
[46] M.H. Healy, L.F. Wieserman, E.M. Arnett, K. Wefers, Langmuir 5 (1989) 114.